Aust. J. Phys., 1985, **38**, 687–704

Reflection of Magnetoionic Waves from a Steep Density Gradient. I Incident Extraordinary Mode

L. M. Hayes

School of Physics, University of Sydney,
Sydney, N.S.W. 2006.

Abstract

Calculations of the relative magnitudes of the four secondary waves produced when a magnetoionic wave encounters an electron density discontinuity within an anisotropic plasma are presented. We identify the different conditions under which each of the secondary waves is the dominant mode, and determine some general properties of the reflection process.

1. Introduction

In recent years, little attention has been paid to the effect of sharp electron density gradients on the propagation of waves within a plasma. Most of the literature on this subject comes from the 1950's and deals with one specific application, that of radio waves reflected from the ionosphere. Bremmer (1949) derived the reflection and transmission coefficients for linearly polarized radio waves striking a sharp boundary between free space and a homogeneous, isotropic ionosphere. This model neglected the Earth's magnetic field, which was first incorporated by Budden (1951) and later by Wait (1957) and Yabroff (1957). The inclusion of an external magnetic field leads to relatively complicated dispersion relations for waves within the ionosphere, and analytic expressions for the reflection and transmission coefficients were obtained by both Budden and Wait only in a special case—specifically the quasi-longitudinal approximation (Budden 1951). Yabroff's description of the phase and magnitude of the reflection and transmission coefficients of radio waves incident upon a sharply bounded ionosphere was exact, but was based on numerical results rather than an analysis of explicit expressions for the reflection coefficients.

Previous calculations of reflection of radio waves from density discontinuities have the advantage that the incident wave is a plane wave propagating in free space and only the transmitted waves are governed by the more complicated plasma dispersion relation. In the present paper, we relax this restriction and consider the general case of an anisotropic plasma comprising two homogeneous regions, each with different electron densities, and a sharp boundary between the regions. The relative magnitudes of the secondary waves generated when a magnetoionic wave encounters such a boundary are calculated, and we determine where significant transfer of energy occurs from the incident wave mode into other modes.

0004-9506/85/050687$02.00

The generation of a weak ordinary mode from an incident extraordinary mode is of particular interest. Auroral kilometric radiation, AKR (Gurnett 1974), which is produced predominantly in the x mode also has a weak o mode component (Benson 1984). Reflection of x mode waves from steep density gradients within the AKR generation region is a possible source of the parasitic o mode. This application is the primary motivation for the present paper; a detailed discussion of it will be presented elsewhere.

The theory of magnetoionic waves is summarized in Section 2, and a brief discussion of the boundary conditions on the wave fields which apply at a sharp density gradient is also given. We comment on the quantity chosen to represent the energy in a plasma wave, and write down the expressions to be included in a numerical code for calculating the reflected and transmitted energy.

In Section 3 we consider the likely effects of the physical parameters of the plasma (e.g. electron density, magnetic field strength and direction) and the wave (e.g. frequency, angle of propagation) on the reflection process, and discuss limitations which are imposed on the analysis by the large number of variables in the problem. We indicate how the results of numerical calculations may be presented to yield the maximum amount of information.

In Section 4 the results for different parameter regions are presented. These apply when the incident wave is in the extraordinary mode—results for the ordinary mode will be given in a later paper.

2. Dispersion Relations and Boundary Conditions

The magnetoionic theory describes cold plasma waves in a homogeneous, anisotropic medium, where the anisotropy is produced by an external magnetic field. The dispersion relation for these waves (known as the Appleton–Hartree formula) was derived by Hartree (1931) and Appleton (1932). Booker (1936) extended this work to include the case of a radio wave obliquely (rather than vertically) incident upon a horizontally stratified ionosphere.

In the present paper we follow the derivation of the magnetoionic dispersion relation given by Budden (1961). Subject to slight changes in notation, the susceptibility matrix in equation (3.24) of Budden (1961) may be substituted into Maxwell's equations to give the following matrix equation for the electric field in the plasma:

$$\begin{bmatrix} M_{11} & M_{12} & M_{13} \\ M_{21} & M_{22} & M_{23} \\ M_{31} & M_{32} & M_{33} \end{bmatrix} \begin{bmatrix} E_x \\ E_y \\ E_z \end{bmatrix} = \mathbf{0}, \tag{1}$$

where

$$M_{11} = (1 - n^2 \cos^2\theta)\, U(U^2 - Y^2) - X(U^2 - l_1^2\, Y^2),$$

$$M_{12} = X(-\mathrm{i}\, l_3\, Y\, U + l_1\, l_2\, Y^2),$$

$$M_{21} = X(\mathrm{i}\, l_3\, Y\, U + l_1\, l_2\, Y^2),$$

$$M_{13} = n^2 \sin\theta \cos\theta\, U(U^2 - Y^2) - X(-\mathrm{i}\, l_2\, Y\, U - l_1\, l_3\, Y^2),$$

$$M_{31} = n^2 \sin\theta \cos\theta\, U(U^2 - Y^2) - X(\mathrm{i}\, l_2\, Y U - l_1\, l_3\, Y^2),$$

$$M_{22} = (1 - n^2)\, U(U^2 - Y^2) - X(U^2 - l_2^2\, Y^2),$$

$$M_{23} = X(-\mathrm{i}\, l_1\, Y U + l_2\, l_3\, Y^2),$$

$$M_{32} = X(\mathrm{i}\, l_1\, Y U + l_2\, l_3\, Y^2),$$

$$M_{33} = (1 - n^2 \sin^2\theta)\, U(U^2 - Y^2) - X(U^2 - l_3^2\, Y^2).$$

Here $X = \omega_p^2/\omega^2$, $Y = \Omega_e/\omega$, $U = 1 - \mathrm{i}\,\nu/\omega$ where ν is the collision frequency (assumed small), and the refractive index n is defined as $|k|\, c/\omega$. The coordinate system used in (1) is chosen as follows. If $\hat{n}$ is the unit vector normal to the surface separating two media of different densities, then let the z axis be in the direction of $\hat{n}$ and let the x and y axes be in the plane of the surface, with the wavevectors of the plasma waves lying in the x–z plane. The direction cosines of the external magnetic field in this coordinate system are l_1, l_2 and l_3, and θ is the angle between the wavevector and the z axis (see Fig. 1).

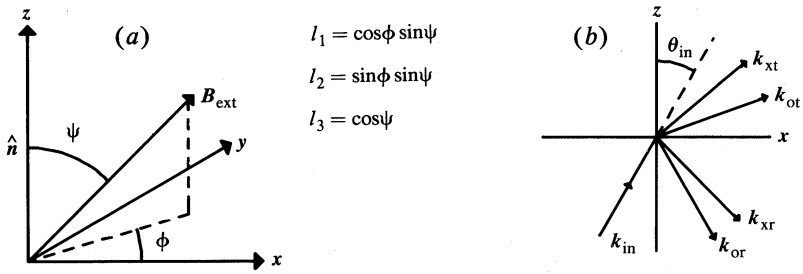

Fig. 1. Diagrams of (*a*) the external magnetic field in the coordinate system chosen, and (*b*) the incident, transmitted and reflected wavevectors.

Evaluating the determinant of the 3×3 matrix in (1) and setting it equal to zero gives the dispersion relation

$$n^4\{U(U^2 - Y^2 - UX) + XY^2(l_3 \cos\theta + l_1 \sin\theta)^2\}$$

$$- n^2\{2(U - X)(U^2 - Y^2 - UX) - XY^2 + XY^2(l_3 \cos\theta + l_1 \sin\theta)^2\}$$

$$+ (U - X)\{(U - X)^2 - Y^2\} = 0. \tag{2}$$

The solutions of (2) have two branches, the o and whistler modes, and the x and z modes [see Melrose (1980), §12.1]. We are only interested in the higher frequency branches, i.e. the o, x and z modes. If we define $q = n \cos\theta$, the normal component of the refractive index, and $r = n \sin\theta$, which is simply Snell's constant, (2) becomes

$$q^4\{U(U^2 - Y^2 - UX) + XY^2 l_3^2\} + q^3 2XY^2 l_1\, l_3\, r$$

$$+ q^2\{XY^2(l_1^2 + r^2 + l_2^2 - l_2^2\, r^2) - 2(U^2 - Y^2 - UX)(U - X - Ur^2)\}$$

$$- q2XY^2 l_1\, l_3\, r(1 - r^2) + \{(U - X)(U - X - Ur^2)^2$$

$$- Y^2(1 - r^2)(U - X - Ur^2) - XY^2 l_1^2\, r^2(1 - r^2)\} = 0, \tag{3}$$

which was first introduced by Booker (1936) and is known as the Booker quartic.

We may solve either (2) or (3) to find the refractive indices of the magnetoionic waves. Equation (2) is a function of wave angle whereas solutions of (3) depend on Snell's constant. In an inhomogeneous medium r, rather than the wave angle, is constant. Hence we use (3) to find the refractive indices $[n = (q^2+r^2)^{\frac{1}{2}}]$ of the secondary waves produced at the density discontinuity.

Equation (3) has four solutions; two which travel in the positive z direction and are referred to as upgoing waves, and two which travel in the negative z direction and are referred to as downgoing waves. If U has a small imaginary part (implying that the waves are weakly collisionally damped), then the solutions of (3) are all complex; two have positive imaginary parts and two have negative imaginary parts. By hypothesis the wave fields are of the form

$$F = F_0 \exp\{-\mathrm{i}\,\omega(rx+qz-ct)/c\}, \tag{4}$$

so a wave with negative imaginary part of q is only damped if it travels in the positive z direction. The appropriate definition of an upgoing wave is therefore one with negative imaginary part of q and a downgoing wave has positive imaginary part of q.

The x, y and z components of the electric field are related by the matrix equation (1), and the magnetic field is given in terms of the electric field by Maxwell's equations. In terms of the x component of the electric field one finds

$$\frac{E_y}{E_x} = \rho_y =$$

$$\frac{\mathrm{i}\{l_1(1-X-q^2)+l_3\,qr\}-l_2\,Y\{l_3(1-q^2)-l_1\,qr\}}{-\mathrm{i}l_2(1-X-l_3^2)-l_2^2 qr\,Y-l_1 l_3\,Y(1-n^2)-qr\{(1-Y^2)(1-n^2)-X\}/XY}, \tag{5}$$

$$\frac{E_z}{E_x} = \rho_z = \frac{\mathrm{i}\{l_1(1-X-q^2)+l_3\,qr\}+l_2\,Y\{l_3(1-q^2)-l_1\,qr\}}{-\mathrm{i}\{l_3(1-X-r^2)+l_1\,qr\}+l_2\,Y\{l_1(1-r^2)-l_3\,qr\}}, \tag{6}$$

$$cB_x/E_x = -q\rho_y, \quad cB_y/E_x = q-r\rho_z, \quad cB_z/E_x = r\rho_y, \tag{7a, b, c}$$

where we have dropped the terms due to collisional damping, i.e. we have set $U = 1$. The field ratios in (5), (6) and (7) may still be complex numbers and it is necessary to take the complex nature of the wave fields into account when the energy and energy flux in the wave are calculated.

Boundary Conditions

Now let us consider what happens when a cold plasma wave travelling in a medium with plasma frequency ω_{p1} strikes a density discontinuity at an angle θ to the normal. A magnetized plasma supports four different wave modes. Therefore one incident wave may generate two reflected and two transmitted waves (see Fig. 1*b*). The electric and magnetic fields of all five waves need to be included in the boundary conditions, which are obtained in the usual way (Jackson 1962). Assuming μ has its free space

value μ_0 on both sides of the boundary, we find that the tangential components of $\boldsymbol{E}$ and $\boldsymbol{B}$ must be continuous across the boundary. If we denote the incident wave by the subscript 'in', the two reflected waves by subscripts 'r1' and 'r2', and the transmitted waves by subscripts 't1' and 't2', the boundary conditions take the form of the matrix equation:

$$\begin{bmatrix} -1 & -1 & 1 & 1 \\ -\rho_{yr1} & -\rho_{yr2} & \rho_{yt1} & \rho_{yt2} \\ q_{r1}\rho_{yr1} & q_{r2}\rho_{yr2} & -q_{t1}\rho_{yt1} & -q_{t2}\rho_{yt2} \\ -q_{r1}+r\rho_{zr1} & -q_{r2}+r\rho_{zr2} & q_{t1}-r\rho_{zt1} & q_{t2}-r\rho_{zt2} \end{bmatrix} \begin{bmatrix} E_{xr1} \\ E_{xr2} \\ E_{xt1} \\ E_{xt2} \end{bmatrix}$$

$$= E_{xin} \begin{bmatrix} 1 \\ \rho_{yin} \\ -q_{in}\rho_{yin} \\ q_{in}-r\rho_{zin} \end{bmatrix} \tag{8}$$

This must be solved to determine the four ratios E_{xr1}/E_{xin}, E_{xr2}/E_{xin}, E_{xt1}/E_{xin} and E_{xt2}/E_{xin} of the x components of the secondary electric fields with respect to the incident field. With (5), (6) and (7), and the solutions of (2) or (3), this completely specifies the four waves generated at the density discontinuity.

Validity of the 'Sharp' Boundary Assumption

An infinite density gradient is of course unphysical, so we should determine how steep a density gradient must be for the boundary conditions assumed above to be valid. Since this is only an order of magnitude calculation, several simplifying assumptions are made:

(1) The incident wavevector is normal to the boundary.

(2) The external magnetic field lies along the boundary and in the plane of incidence.

(3) The electron density within the transition region varies linearly with distance and the electric fields are functions of z only.

The first two assumptions imply that one mode has an electric field lying in the plane of incidence while the other mode's electric field is perpendicular to the plane of incidence; hence the equations describing the variation of the electric fields with distance separate into two independent second order differential equations. In the uniform plasma on either side of the boundary the solutions of these equations are plane waves, while within the boundary series solutions may be found for the differential equations. By matching the plane waves to the series solutions at both edges of the transition region, expressions for the electric fields on either side of the boundary may be obtained. Details of the calculation of these fields are given in the Appendix.

In the limit of an infinitely thin transition region the tangential electric fields on either side of the boundary are equal. Let us assume that we may make this

approximation if the electric fields (A12a) and (A12b) in the Appendix differ by no more than 10%, i.e.

$$|E| \text{ (incident region)} - |E| \text{ (final region)} < 0{\cdot}1\,|E| \text{ (incident region)}. \tag{9}$$

Then from the Appendix the maximum boundary width d satisfies the condition

$$d < \lambda_2(X_2 - X_1)/20\pi\,. \tag{10}$$

Hence the boundary is of the order of a wavelength λ_2 thick.

Estimation of Wave Energy

Finally, we must determine the most appropriate way to estimate the relative amount of energy in plasma waves. One simple choice would be the energy in the electric field $|E|^2$. Another possibility is the component of the Poynting vector normal to the boundary S_z. This has the advantage that it is always zero when the wave is evanescent and S_z calculated at the boundary gives an estimate of the energy flux a distant observer would see. However, for an evanescent wave $|E|^2$ is not zero at the boundary and must be calculated at large distances from the boundary. Furthermore, S_z must be continuous across the boundary and this condition may be used to check the accuracy of numerical calculations. For these reasons S_z rather than $|E|^2$ is used as a measure of the energy in each wave and henceforth the term 'energy' refers to the energy flux normal to the boundary. In fact numerical calculations indicate that, for propagating waves, S_z is roughly proportional to $|E|^2$.

By using the definition of the Poynting vector for complex wave fields,

$$S = \mathrm{Re}(E) \times \mathrm{Re}(H), \tag{11}$$

the time-averaged component of S normal to the boundary for any one wave is given by

$$S_z \propto |E_x|^2\{\mathrm{Re}(q)(1+|\rho_y|^2) - \mathrm{Re}(r\rho_z)\}, \tag{12}$$

where q is one of the solutions of (3), ρ_y and ρ_z are given by (5) and (6), r is Snell's constant, and E_x is found by solving (8).

The fraction of energy going into each wave is taken to be $S_z/S_{z\mathrm{in}}$ and it is this quantity (referred to simply as S_z), evaluated for each of the two reflected and two transmitted waves, which we study. The refractive indices of the transmitted waves may be complex even though the incident wave has a real refractive index. Let us consider the solution of (3) for the special case of the magnetic field in the x–y plane (and $U = 1$):

$$q^2 = 1 - X - r^2 - XY^2(1 + l_1^2 r^2)/2(1 - X - Y^2)$$
$$\pm XY\{l_1^2 r^2(1-X) + \tfrac{1}{4}Y^2(1 - l_1^2 r^2)^2\}^{\frac{1}{2}}/(1 - X - Y^2). \tag{13}$$

Snell's constant must be real for both incident and transmitted waves, so the values of q^2 for the transmitted waves are complex conjugates when the expression within the square root in (13) is negative, i.e.

$$\omega_{p2}^2 > \omega^2 + \Omega_e^2(1 - l_1^2 r^2)^2/4 l_1^2 r^2, \tag{14}$$

where ω_{p2} refers to the plasma frequency in the second medium, and r is a function of Ω_e, ω, l_1 and ω_{p1}. Since $\tan\theta = r/q$, these waves propagate at complex angles. However, S_z for each wave is zero and there is no net energy flux across the boundary in this case.

3. Presentation of Data

There are two main problems associated with describing the waves that are transmitted through or reflected from a density discontinuity within a plasma. The first arises from the complicated forms not only of the dispersion relations but also of the expressions for the reflection coefficients. In general, it is not possible to analytically determine the relative amounts of energy in the secondary waves produced by the reflection, and so the problem must be studied numerically. However, this is also difficult because there are so many physical parameters on which the reflection and transmission coefficients depend that any numerical analysis cannot completely determine the effect on the coefficients as these parameters vary.

The results we obtain are in the form of graphs of the z component of the Poynting vector against one of the variable parameters. The possible physical variables in this problem are ω, ω_{p1}, ω_{p2}, Ω_e, l_1, l_2, l_3, $\sin\theta_{in}$ and the type of incident mode which may be o or x. In this paper we concentrate on the case of an incident x mode.

In most physical applications of this reflection theory one would expect the external magnetic field to be in the plane of the boundary between the two different density regions. This corresponds to $l_3 = 0$, and with this assumption only one parameter l_1 is needed to describe the direction of the magnetic field. The choice $l_3 = 0$ also has the advantage that the quartic equation for q reduces to a quadratic in q^2 which may be solved simply.

We have chosen to normalize all frequencies with respect to ω_{p1} so there are five quantities to be considered in numerical calculations: ω/ω_{p1}, ω_{p2}/ω_{p1}, Ω_e/ω_{p1}, l_1 and $\sin\theta_{in}$.

The variation of S_z with ω/ω_{p1} is much more complicated than its variation with any of the other parameters (which is not surprising when the behaviour of the refractive index as a function of frequency is considered), and since this can only be described adequately by taking a large number of examples, we have chosen to plot S_z as a continuous function of ω/ω_{p1}. The effect of varying the other parameters must then be determined by comparing many different graphs of S_z against ω/ω_{p1}, where one of the other parameters varies from graph to graph and the remaining quantities stay the same. If the trends caused by varying the other parameters are smooth enough then this analysis gives an adequate indication of those trends.

Even after setting $l_3 = 0$ we are still left with five free parameters, three of which are between 0 and ∞, and the remaining two are between -1 and 1. After considering what parameter ranges are likely to have specific applications and what ranges are logistically feasible to study, the following choices were made:

$1 < \omega/\omega_{p1} < 20$. The o mode cut-off occurs at $\omega = \omega_{p1}$ and we are only interested in magnetoionic modes at frequencies above this. For large frequencies the refractive indices for the different modes approach limiting values and the four S_z ratios also approach asymptotic limits, so it is not necessary to take ω/ω_{p1} much larger than 20. Often we only consider $\omega/\omega_{p1} < 10$. However, for this to be an

adequate representation of frequency space, the upper limits of both ω_{p2}/ω_{p1} and Ω_e/ω_{p1} must also be less than 20.

$1 < \omega_{p2}/\omega_{p1} < 10$. When ω_{p2} is less than ω_{p1} the energy in the incident wave is transferred almost completely to the transmitted wave in the same mode. The reflection and transmission coefficients only begin to show interesting behaviour for $\omega_{p2}/\omega_{p1} > 1$ (i.e. when the second medium has a higher electron density than the first medium). The upper limit of the plasma frequency ratio has been chosen to be less than 20, but still corresponds to a density jump of two orders of magnitude.

$0 < \Omega_e/\omega_{p1} < 1$. In most physical situations the magnetic field is relatively weak and Ω_e/ω_p is less than 1 in both media. This case will be considered first.

$1 < \Omega_e/\omega_{p1} < 10$. This limit occurs in at least one important example—the generation of AKR. An upper limit of 10, which seems to be fairly typical of the AKR generation region, has been chosen.

$0 < l_1 < 1$. When l_3 equals zero, the reflection and transmission coefficients are symmetric in both l_1 and l_2, so it is only necessary to consider the magnetic field lying in one quadrant of the x–y plane; $l_1 = 0$ corresponds to the magnetic field perpendicular to the plane of incidence, and $l_1 = 1$ corresponds to the magnetic field in the plane of incidence.

$0 < \sin\theta_{in} < 1$. Again because of the symmetry of the problem, only angles of incidence between 0° and 90° need be considered.

4. Results

Some of the results in this section are illustrated by graphs of S_z against frequency. The examples chosen are all for the case $\Omega_e/\omega_{p1} > 1$, and in a later paper these results will be used to study the polarization of AKR. The graphs should be interpreted as follows. The upper graphs in each figure give the fraction of energy going into the two reflected modes while the lower graphs show the transmitted modes. The o mode is represented by a dashed curve and the x mode by a solid curve. Each pair of upper and lower graphs in Figs 4–7 forms part of a series of graphs, and one of the four parameters ω_{p2}/ω_{p1}, Ω_e/ω_{p1}, l_1 or $\sin\theta_{in}$ varies for each pair of graphs in the series, while the remaining three parameters are the same. Before presenting detailed results we discuss several features common to all the graphs of S_z obtained.

Our choice of $l_3 = 0$ for the external magnetic field implies that the regions where the normal energy flux of a mode is zero are regions where the normal component q of the refractive index is imaginary. (We exclude the case of q components with real and imaginary parts which was considered in the previous section.) To see this, consider the expression for S_z when $l_3 = 0$:

$$S_z \propto \mathrm{Re}(q)(1+|\rho_y|^2) - r\,\mathrm{Re}(\rho_z), \tag{15}$$

where

$$\rho_z = \{\mathrm{i}(1-X-q^2) + q l_2\, Y r\}/\{-\mathrm{i}\, qr - l_2\, Y(1-r^2)\}. \tag{16}$$

If q is real then ρ_z has a non-zero real part, and in general S_z is non-zero. However, if q is imaginary so is ρ_z, and S_z must then be zero. The close relation between q^2 and S_z is illustrated in Fig. 2.

The x mode cut-off frequencies (i.e. where $q^2 = 0$) in both the incident and final plasma are important in determining the boundaries of frequency regions in which

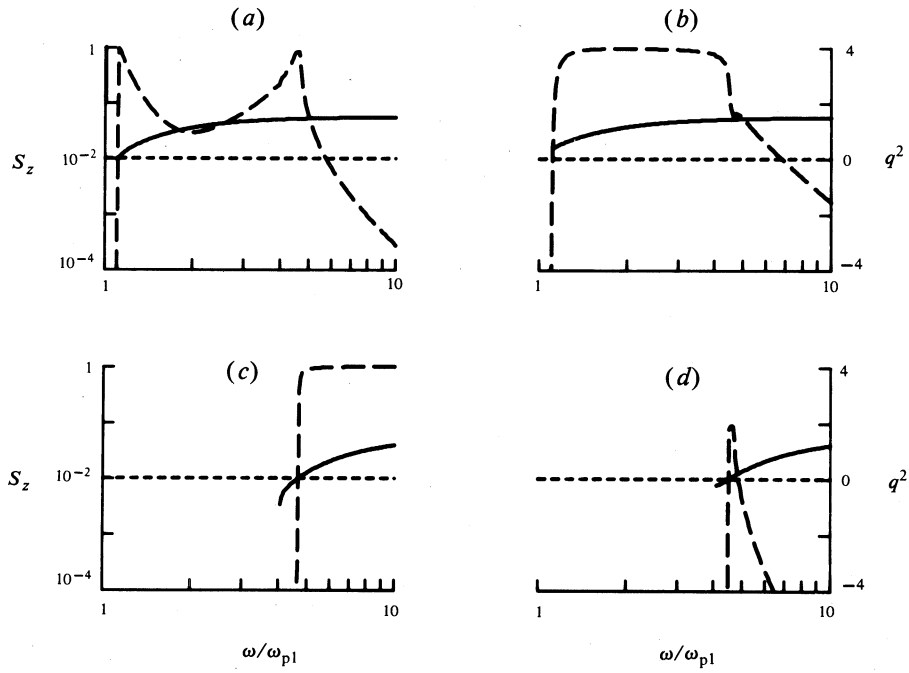

Fig. 2. Graphs showing q^2 (solid curve) and the corresponding normal Poynting flux S_z (dashed curve) for (*a*) the reflected x mode, (*b*) the reflected o mode, (*c*) the transmitted x mode and (*d*) the transmitted o mode. Graphs are for $\omega_{p2}/\omega_{p1} = 4$, $\Omega_e/\omega_{p1} = 0{\cdot}2$, $l_1 = 1$ and $\theta_{in} = 30°$.

different types of reflected and transmitted modes occur. From (3) the x mode cut-off occurs when

$$(1-X)(1-X-r^2)^2 - Y^2(1-r^2)(1-X-r^2+Xr^2l_1^2) = 0. \tag{17}$$

For the simple case $l_1 = 1$, the cut-off frequency is

$$\omega_{ci} = \tfrac{1}{2}\Omega_e + \{\tfrac{1}{4}\Omega_e^2 + \omega_{pi}^2/(1-r^2)\}^{\frac{1}{2}}, \qquad i = 1,2, \tag{18}$$

where r is $\sin\theta_{in}$ multiplied by one of the solutions of (2), which is a function of ω_{p1}, Ω_e and θ_{in}. Because (2) and (3) must give consistent results, in the first region the incident mode cut-off is simply

$$\omega_{c1} = \tfrac{1}{2}\Omega_e + (\tfrac{1}{4}\Omega_e^2 + \omega_{p1}^2)^{\frac{1}{2}}, \tag{19}$$

which increases with increasing magnetic field strength. In the second region the cut-off is

$$\omega_{c2} = \tfrac{1}{2}\Omega_e + [\tfrac{1}{4}\Omega_e^2 + \omega_{p2}^2/\{1 - r^2(\omega_{p1}, \Omega_e, \theta_{in})\}]^{\frac{1}{2}}, \tag{20}$$

which is a function of the density change and angle of incidence as well as the magnetic field. While ω_{c2} obviously increases with increasing density change, its dependence

on the other parameters is not as clear. However, in general ω_{c2} increases with increasing angle of incidence and magnetic field strength, and is almost independent of the magnetic field direction.

One would expect the shapes of the graphs of S_z as a function of frequency for different modes to be related—the transfer of most of the energy into one of the modes means that little energy is transferred to the other modes. It is nevertheless interesting that at higher frequencies the reflected and transmitted o mode curves are similar, although both are weak modes (see Figs 2*b* and 2*d*).

With these preliminary remarks let us consider the effect of different parameters on the reflection coefficients.

Summary of Results—Small Magnetic Field

The general characteristics of the reflected and transmitted modes when $\Omega_e/\omega_{p1} < 1$ are summarized:

(*a*) The transmitted x mode is dominant (i.e. the density gradient has very little effect) for small and moderate angles of incidence and at frequencies higher than the x mode cut-off in the second region.

(*b*) An incident x mode may produce a transmitted z mode at frequencies below ω_{c2}. The strength of this mode decreases as the angle of incidence increases, as the magnetic field strength decreases, or as the density ratio increases.

(*c*) There is little transmitted o mode generated, with the maximum transfer of energy into this mode occurring when there is no transmitted x or z mode. This mode is strongest when the magnetic field is weak or is near the plane of incidence, or when the density ratio is large.

(*d*) Significant reflection only occurs below ω_{c2} or at large angles of incidence. The reflected wave may be predominantly o or x mode, with the ratio of reflected o to reflected x mode increasing as the density ratio increases, the magnetic field strength decreases or it becomes aligned with the plane of incidence, or as angles of incidence around 45° are reached.

Summary of Results—Large Magnetic Field or Small Initial Plasma Density

This is the parameter region which is relevant to the study of AKR, and the effects on S_z of varying each of the five plasma or wave parameters when $\Omega_e/\omega_{p1} > 1$ are illustrated in Figs 3–7. As one would expect, many of the results for $\Omega_e/\omega_{p1} > 1$ are similar to results when $\Omega_e/\omega_{p1} < 1$. The frequencies where S_z is zero are still determined by zeros and infinities of q^2. There is an even closer correspondence between the behaviour of the reflected and transmitted o modes. The results for the transmitted modes when $\Omega_e/\omega_{p1} < 1$ [i.e. (*a*), (*b*) and (*c*) above] are valid for all values of Ω_e/ω_{p1}. The only further comment which can be made is that the size of the o modes depends more strongly on the ratio Ω_e/ω_{p1} when it is greater than one.

However, the behaviour of the reflected modes is slightly different for large magnetic fields, and is summarized below.

(*a'*) The reflected waves produced are different above and below the incident x mode cut-off ω_{c1}, although the x mode is usually the stronger mode at all frequencies.

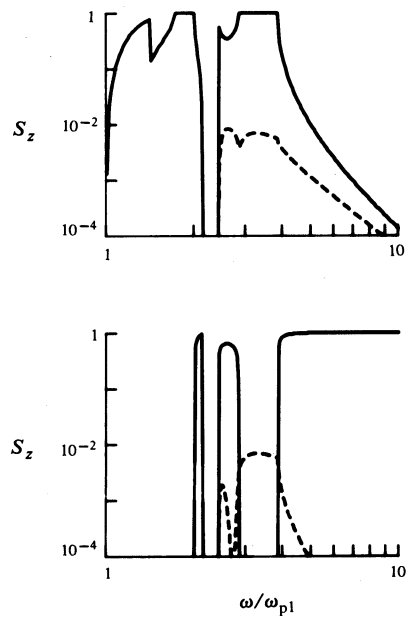

Fig. 3. Graphs of S_z against frequency for the two reflected modes (upper) and the two transmitted modes (lower). Dashed curves correspond to o modes and solid curves to x modes. Graphs are for $\omega_{p2}/\omega_{p1} = 2$, $\Omega_e/\omega_{p1} = 2$, $l_1 = 1$ and $\theta_{in} = 45°$. The following observations are noted: (i) The asymptotic behaviour at large frequencies and the dependence of all the transmitted modes on frequency are the same as for $\Omega_e/\omega_{p1} < 1$. (ii) Again significant reflection only occurs below the x mode cut-off in the denser region ω_{c2} but the reflected o mode is almost invariably weaker than the reflected x mode, unless the frequency is low and the incident mode is z rather than x. (iii) The incident mode is in fact a z mode over a much wider range of frequencies above ω_{p1} than when $\Omega_e/\omega_{p1} < 1$.

(b') Between ω_{c1} and ω_{c2} the reflected o mode becomes stronger if the density ratio increases, the magnetic field decreases or lies in the plane of incidence, or the angle of incidence increases.

(c') Below ω_{c1}, the reflected z mode is weaker at small angles of incidence or for large magnetic fields, and may be weaker for smaller density ratios. There may or may not be a reflected o mode.

5. Discussion

Although the behaviour of waves reflected from and transmitted through a sharp density change is difficult to study analytically, careful examination of numerical calculations allows one to identify several important features of the reflection process. For the case considered here of an incident extraordinary mode and the magnetic field in the plane of the boundary between the two regions of different density, we have shown that the reflected modes may be dominated by the o rather than the x mode, particularly at frequencies just above the plasma frequency of the incident region.

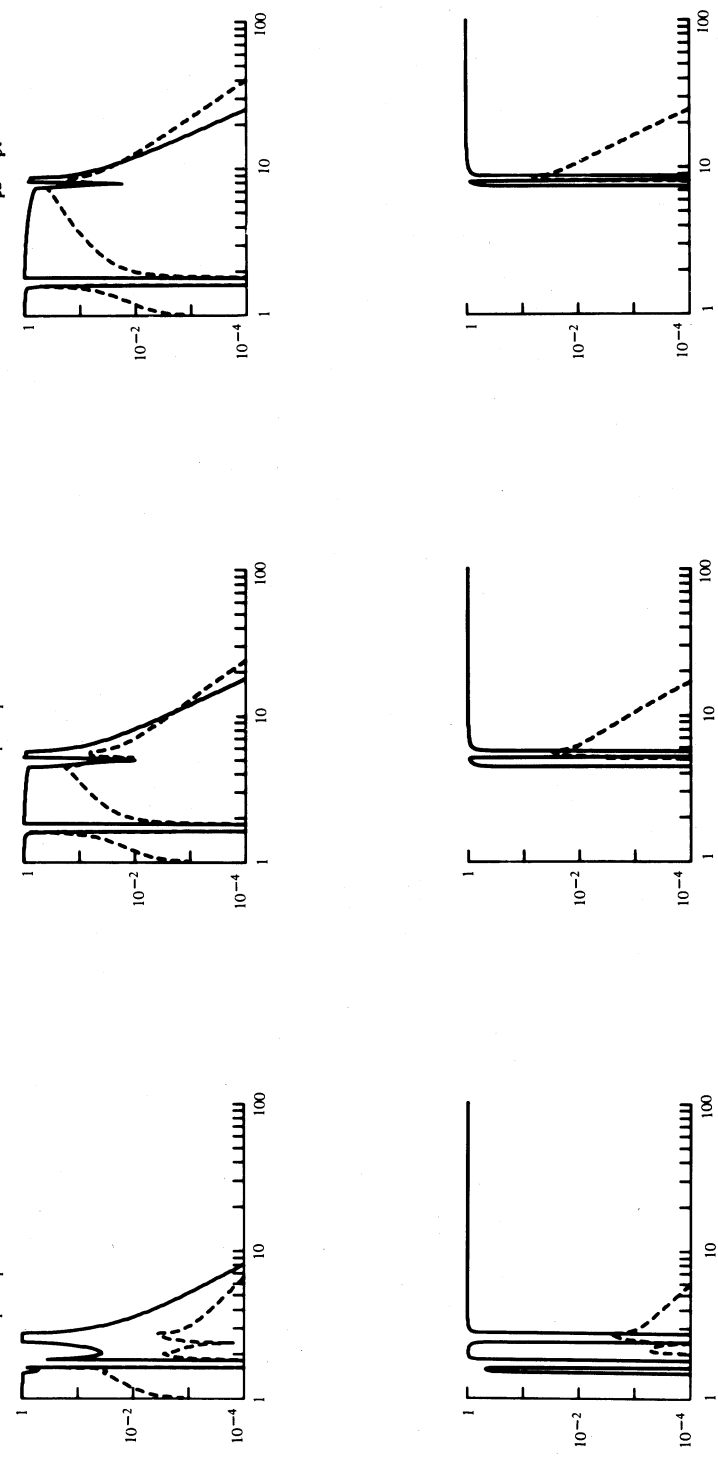

Fig. 4. Graphs of S_z against frequency for ω_{p2}/ω_{p1} changing, $\Omega_e/\omega_{p1} = 1{\cdot}25$, $l_1 = 0{\cdot}707$ and $\theta_{in} = 5°$. As ω_{p2}/ω_{p1} increases: (i) The transmitted x and z modes are seen only at higher frequencies while the transmitted z mode propagates over a smaller frequency range. (ii) The transmitted o mode propagates at higher frequencies, becoming stronger, but over a smaller frequency range. (iii) The range of frequencies over which the incident mode is reflected becomes larger, with the reflected o mode becoming stronger.

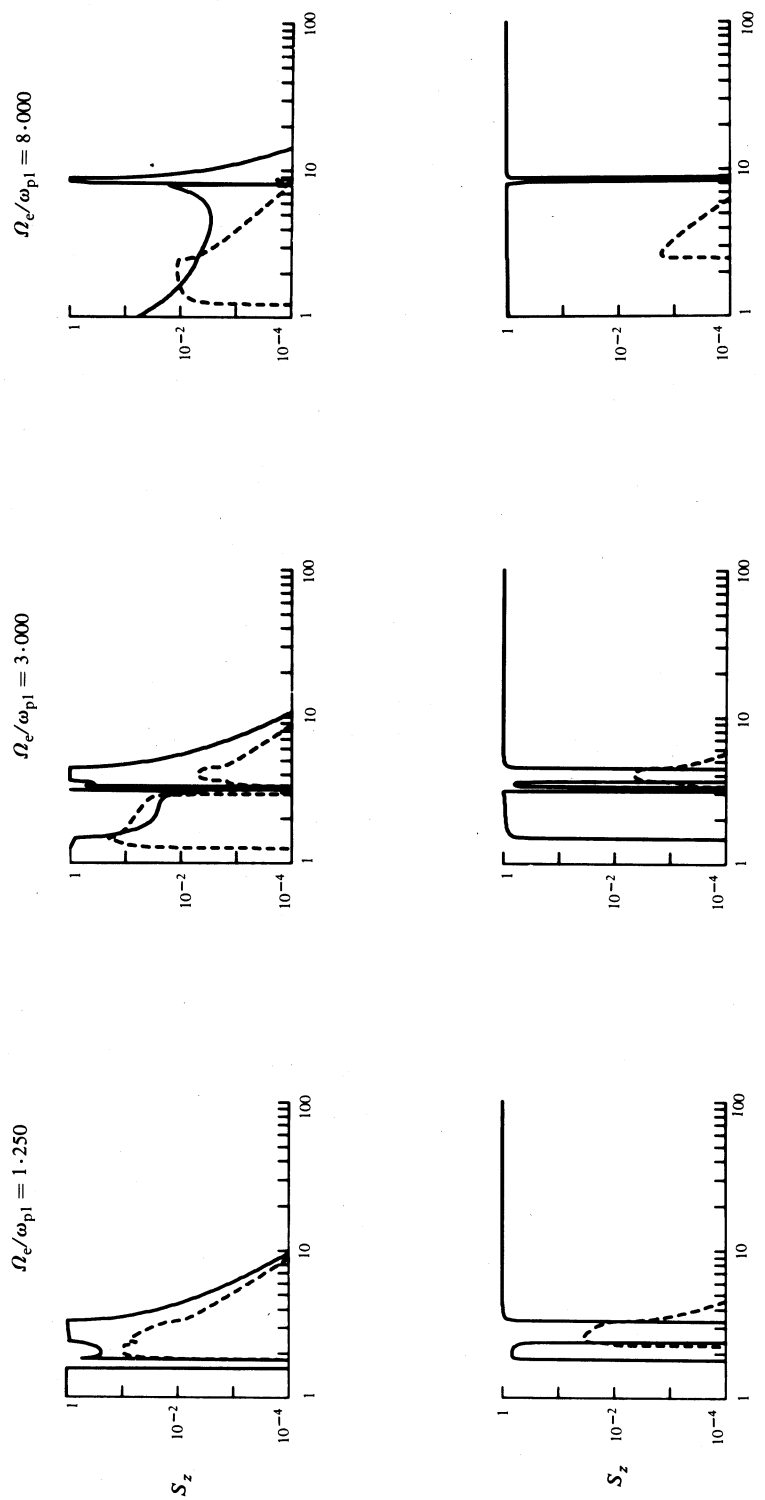

Fig. 5. Graphs of S_z against frequency for Ω_e/ω_{p1} changing, $\omega_{p2}/\omega_{p1} = 2$, $l_1 = 0{\cdot}707$, $\theta_{in} = 45°$. As Ω_e/ω_{p1} increases: (i) The transmitted z mode is observed over a much wider frequency range and the strength of the transmitted o mode decreases appreciably. (ii) The reflected x mode also decreases for frequencies above ω_{c2}, although at lower frequencies there are no consistent trends in the size of the x mode. (iii) Most of the energy reflected is x mode, but it is seen over a decreasing range of frequencies. When the incident mode is a z mode, the reflected wave, as well as becoming weaker, contains o and z modes of roughly equal strength.

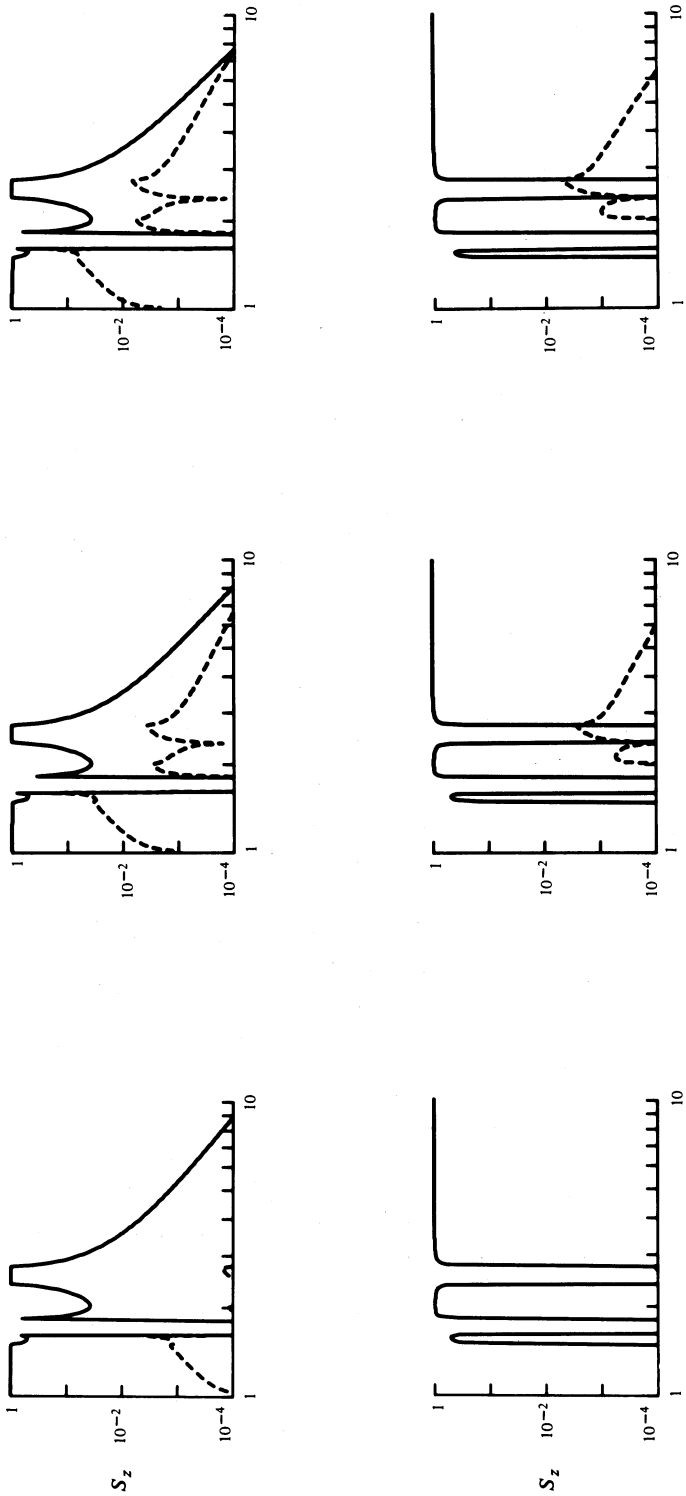

Fig. 6. Graphs of S_z against frequency for l_1 changing, $\omega_{p2}/\omega_{p1} = 2$, $\Omega_e/\omega_{p1} = 1{\cdot}25$ and $\theta_{in} = 5°$. As l_1 increases: (i) There is little change in the strength of the x modes, but the o modes become stronger. (ii) Below ω_{c1} (i.e. incident z mode), if the reflected o mode exists it may or may not be the dominant reflected mode.

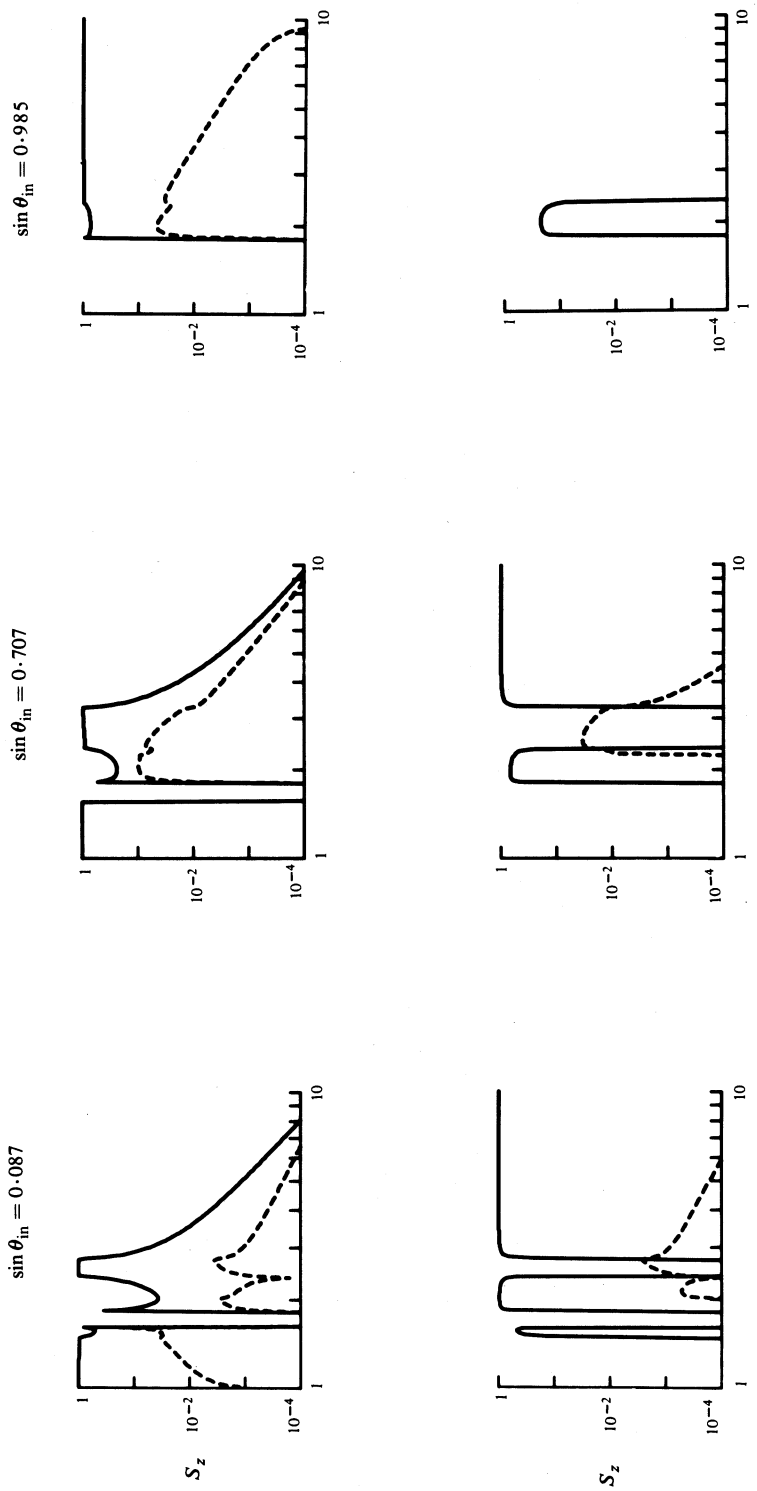

Fig. 7. Graphs of S_z against frequency for θ_{in} changing, $\omega_{p2}/\omega_{p1} = 2$, $\Omega_e/\omega_{p1} = 1{\cdot}25$ and $l_1 = 0{\cdot}707$. As θ_{in} increases: (i) The transmitted x mode again becomes evanescent, although there still appears to be some z mode. (ii) Both o modes at first become stronger, then decrease, sometimes becoming evanescent. (iii) The reflected x and z modes are dominant at large angles of incidence.

We have also found that strong transmitted z modes occur, and of course under many conditions the incident wave is almost completely reflected. Parasitic o modes are invariably present, although they may be many orders of magnitude weaker than the x mode. In general they become stronger with increasing density ratio, decreasing magnetic field strength, or for incident angles around 45°.

The generation of secondary modes in plasmas is usually considered to be the result of wave interactions, or mode coupling in a slowly varying medium. Steeper density gradients, when invoked, have been used to account for wave ducting or confinement (Duncan 1979; Calvert 1982). However, we have seen that they also produce radiation propagating in a different mode from the incident wave, and under appropriate physical conditions reflections from these gradients may be the dominant mechanism generating secondary modes.

Abrupt density changes have been observed in the source region of AKR (Benson and Akasofu 1984), and it is likely they also exist in the solar corona (Pick *et al.* 1979). Since the fraction of incident energy going into secondary reflected and transmitted modes is relatively sensitive to some of the plasma and wave parameters, from observations of these regions it should be possible to determine if some of the magnetoionic waves which are seen are the result of a sharp density gradient within that region.

Acknowledgments

I wish to thank Professor D. B. Melrose for guiding the initial work on reflection of magnetoionic waves and for many helpful discussions.

References

Abramowicz, M., and Stegun, I. A. (1972). 'Handbook of Mathematical Functions' (Dover: New York).
Appleton, E. V. (1932). *J. Inst. Electr. Eng.* **71**, 642.
Benson, R. F. (1984). *Radio Sci.* **19**, 543.
Benson, R. F., and Akasofu, S. (1984). *Radio Sci.* **19**, 527.
Booker, H. G. (1936). *Proc. R. Soc. London* A **155**, 235.
Bremmer, H. (1949). 'Terrestrial Radio Waves' (Elsevier: New York).
Budden, K. G. (1951). *Philos. Mag.* **42**, 833.
Budden, K. G. (1961). 'Radio Waves in the Ionosphere' (Cambridge Univ. Press).
Calvert, W. (1982). *J. Geophys. Res.* **87**, 8199.
Duncan, R. A. (1979). *Sol. Phys.* **63**, 389.
Gurnett, D. A. (1974). *J. Geophys. Res.* **79**, 4227.
Hartree, D. R. (1931). *Proc. Cambridge Philos. Soc.* **27**, 143.
Jackson, J. D. (1962). 'Classical Electrodynamics' (Wiley: New York).
Melrose, D. B. (1980). 'Plasma Astrophysics' (Gordon and Breach: New York).
Pick, M., Trottet, G., and MacQueen, R. M. (1979). *Sol. Phys.* **63**, 369.
Wait, J. R. (1957). *J. Geophys. Res.* **62**, 43.
Yabroff, I. W. (1957). *Proc. Inst. Radio Eng.* **45**, 750.

Appendix

The equations relating the electric and magnetic fields of a plasma wave in the coordinate system of Fig. 1*a* are

$$\partial E_y/\partial z = \mathrm{i}\omega B_x, \qquad \partial B_y/\partial z = \mathrm{i}\omega\{(P_{11}-1)E_x + P_{12}E_y + P_{13}E_z\}/c^2, \qquad \text{(A1a, b)}$$

$$\mathrm{i}\,k_x\,E_z - \partial E_x/\partial z = \mathrm{i}\,\omega B_y, \tag{A2a}$$

$$\mathrm{i}\,k_x\,B_z - \partial B_x/\partial z = \mathrm{i}\,\omega\{P_{21}\,E_x + (P_{22}-1)E_y + P_{23}\,E_z\}/c^2, \tag{A2b}$$

$$-\mathrm{i}\,k_x\,E_y = \mathrm{i}\,\omega B_z, \quad -\mathrm{i}\,k_x\,B_y = \mathrm{i}\,\omega\{P_{31}\,E_x + P_{32}\,E_y + (P_{33}-1)E_z\}/c^2, \tag{A3a, b}$$

where

$$\boldsymbol{P} = \frac{X}{1-Y^2}\begin{bmatrix} 1-l_1^2\,Y^2 & \mathrm{i}\,Y l_3 - Y^2 l_1\,l_2 & -\mathrm{i}\,Y l_2 - Y^2 l_1\,l_3 \\ -\mathrm{i}\,Y l_3 - Y^2 l_1\,l_2 & 1-l_2^2\,Y^2 & \mathrm{i}\,Y l_1 - Y^2 l_3\,l_2 \\ \mathrm{i}\,Y l_2 - Y^2 l_1\,l_3 & -\mathrm{i}\,Y l_1 - Y^2 l_3\,l_2 & 1-l_3^2\,Y^2 \end{bmatrix} \tag{A4}$$

and we have used the fact that the plasma varies only in the z direction.

Under the assumption of vertical incidence ($k_x = 0$), and with $l_1 = 1$, $l_2 = l_3 = 0$, (A3) and (A4) reduce to two independent second order differential equations:

$$c^2\,\partial^2 E_x/\partial z^2 + \omega^2(1-X)E_x = 0, \tag{A5a}$$

$$c^2\,\partial^2 E_y/\partial z^2 + \omega^2\{1 - X - XY^2/(1-X-Y^2)\}E_y = 0. \tag{A5b}$$

Now let us assume the density profile is described by

$$X = X_1 + \Delta X z/d,$$

where $X_i = \omega_{\mathrm{p}i}^2/\omega^2$, $\Delta X = X_2 - X_1$ (typically between 1 and 10), and d is the width of the boundary region. Changing the variable z in (A5a) to $\alpha = 1-X$, and in (A5b) to $\beta = 1-X-Y^2$, we find

$$\partial^2 E_x/\partial\alpha^2 + (\omega d/c\Delta X)^2\alpha E_x = 0, \tag{A6a}$$

$$\partial^2 E_y/\partial\beta^2 + (\omega d/c\Delta X)^2(\beta + p_1 + p_2/\beta)E_y = 0, \tag{A6b}$$

where $p_1 = 2Y^2$ and $p_2 = Y^2(Y^2-1)$.

In the boundary area, the series solutions of (A6a) are related to the Airy function (Abramowicz and Stegun 1972, §10.4), and have the forms

$$E_{x1}(\alpha) = 1 - \tfrac{1}{6}(\omega d/c\Delta X)^2\alpha^3 + \tfrac{1}{180}(\omega d/c\Delta X)^4\alpha^6 + \ldots, \tag{A7a}$$

$$E_{x2}(\alpha) = \alpha - \tfrac{1}{12}(\omega d/c\Delta X)^2\alpha^4 + \tfrac{1}{504}(\omega d/c\Delta X)^4\alpha^7 + \ldots. \tag{A7b}$$

Series solutions for (A6b) have the more complicated forms

$$\begin{aligned} E_{y1}(\beta) = {} & \beta - (\omega d/c\Delta X)^2(\tfrac{1}{2}p_2\,\beta^2 + \tfrac{1}{6}p_1\,\beta^3 + \tfrac{1}{12}\beta^4) \\ & + (\omega d/c\Delta X)^4(\tfrac{1}{12}p_2^2\,\beta^3 + \ldots) + \ldots, \end{aligned} \tag{A8a}$$

$$\begin{aligned} E_{y2}(\beta) = {} & -(\omega d/c\Delta X)^2 p_2\,\log(\beta)\,E_{y1}(\beta) \\ & + 1 + (\omega d/c\Delta X)^2(p_2\,\beta - \tfrac{1}{2}p_1\,\beta^2 - \tfrac{1}{6}\beta^3) \\ & - (\omega d/c\Delta X)^4(\tfrac{5}{4}p_2^2\,\beta^2 + \ldots) + \ldots. \end{aligned} \tag{A8b}$$

The tangential electric and magnetic fields must be continuous at the edges of the boundary region, $z = 0$ and $z = d$. From (A1a) and (A2a) we have

$$B_x = -\mathrm{i}\, c/\omega\ \partial E_y/\partial z\,, \qquad B_y = \mathrm{i}\, c/\omega\ \partial E_x/\partial z\,. \tag{A9a,b}$$

Hence we require the fields (A7) and (A8) and their derivatives to be continuous at the boundary edges. The tangential electric fields on either side of the boundary region may be written

$$\text{Incident region} \qquad E = E_i\{\exp(-\mathrm{i}\, n_1\, z) + R\, \exp(\mathrm{i}\, n_1\, z)\}\,, \tag{A10}$$

$$\text{Final region} \qquad E = E_i\, T\, \exp(-\mathrm{i}\, n_2 z)\,, \tag{A11}$$

where n_1 and n_2 are the refractive indices in the two regions, R and T are complex reflection and transmission coefficients, and we have temporarily dropped the x and y subscripts. The boundary conditions become

$$E_i(1+R) = A\, E_1(z=0) + B\, E_2(z=0)\,, \tag{A12a}$$

$$A\, E_1(z=d) + B\, E_2(z=d) = E_i\, T\, \exp(-\mathrm{i}\, n_2\, d)\,, \tag{A12b}$$

$$-\mathrm{i}\, n_1\, E_i(1-R) = A\, E_1'(z=0) + B\, E_2'(z=0)\,, \tag{A13a}$$

$$A\, E_1'(z=d) + B\, E_2'(z=d) = -\mathrm{i}\, n_2\, E_i\, T\, \exp(-\mathrm{i}\, n_2\, d)\,, \tag{A13b}$$

where $f' \equiv \mathrm{d}f/\mathrm{d}z$.

We assume that the boundary conditions may be approximated by those at a sharp density change if the difference in the fields outside the boundary region is less than 10%, i.e.

$$\{E_i(1+R) - E_i\, T\, \exp(-\mathrm{i}\, n_2\, d)\}/E_i(1+R) < 0{\cdot}1\,. \tag{A14}$$

Solving (A12) and (A13) for R and T, then substituting them into (A14) we get

$$1 - \frac{E_2'(z=d)\, E_1(z=d) - E_1'(z=d)\, E_2(z=d)}{D_2\, E_1(z=0) - D_1\, E_2(z=0)} < 0{\cdot}1\,, \tag{A15}$$

where $D_1 = E_1'(z=d) + \mathrm{i}\, n_2\, E_1(z=d)$ and $D_2 = E_2'(z=d) + \mathrm{i}\, n_2 E_2(z=d)$.

We are interested in the limit of a narrow boundary, so we retain only terms of lowest order in d in (A7) or (A8). Substituting these terms into (A15) gives

$$d < c\Delta X/10 n_2\, \omega \tag{A16}$$

for both the x and y fields. We have $c/n_2\, \omega = \lambda_2/2\pi$, so the maximum boundary width for which the approximation of a sharp boundary is valid is

$$d < \lambda_2\, \Delta X/20\pi\,. \tag{A17}$$

Manuscript received 30 January, accepted 1 July 1985